Proceedings of the DIS'2004, Štrbské Pleso, Slovakia

BARYON-ANTIBARYON PAIR PRODUCTION IN TWO-PHOTON COLLISIONS AT LEP

KLAUS FREUDENREICH
Labor für Hochenergiephysik, ETH Hönggerberg
CH-8093 Zürich, Switzerland
E-mail: Klaus.Freudenreich@cern.ch

The production of p $\bar{\text{p}}$, $\Lambda\overline{\Lambda}$ and $\Sigma^0\overline{\Sigma^0}$ pairs is studied in two-photon collisions at LEP. These data allow to study the partonic substructure of baryons. The data from the LEP experiments, L3 and OPAL, are compared to experiments at lower c.m. energies and to theoretical models. The three quark model predicts in all cases a too low cross section while the quark-diquark model and a handbag model (for the strange baryon pairs) describe the data well.

1 Introduction

The measurement of the process $e^+e^- \to e^+e^-\gamma^*\gamma^* \to e^+e^-X$, where γ^* denotes a virtual photon, allows to extract the cross section $\gamma\gamma \to X$.

The $\gamma\gamma \to$ baryon-antibaryon cross section has been calculated using the hard scattering approach of Brodsky and Lepage [1]. In this calculation the process is factorized into a perturbative amplitude for $\gamma\gamma \to q\,\overline{q}$ and a non-perturbative amplitude for $q\,\overline{q} \to$ baryon-antibaryon.

For this non-perturbative amplitude three possibilities are considered (Fig. 1):

1. using three-quark distribution functions [2,3]
2. describing the partonic structure of the baryons by a quark-diquark system [4]
3. using the so-called handbag model [5].

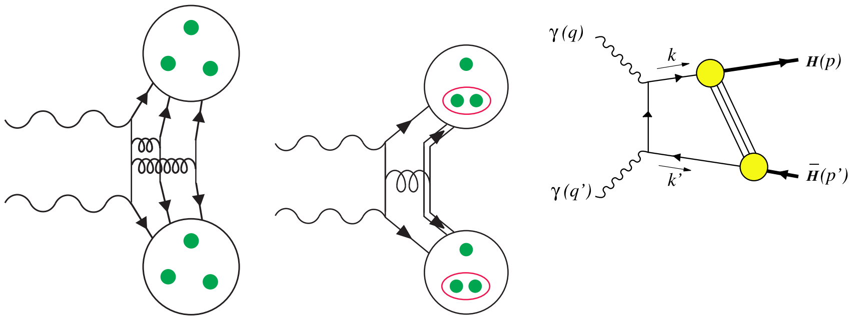

Figure 1. Baryon-antibaryon production in the three quark model (left), in the quark-diquark model (center) and in the handbag model (right).

When comparing the graph with three quarks in the baryon (Fig. 1 left) with the quark-diquark one (Fig. 1 center) one notices that the quark-diquark amplitude is of lower order in α_s and hence should yield a larger cross section.

In the handbag model the annihilation of two photons into a baryon anti-baryon pair is factorized into a hard $\gamma\gamma \to \mathrm{q}\,\overline{\mathrm{q}}$ subprocess and a soft distribution amplitude $A(\mathrm{B}\ \overline{\mathrm{B}})$ for the strange baryon-antibaryon pair. This amplitude is related to the proton-antiproton amplitude $A(\mathrm{p}\ \overline{\mathrm{p}})$ via:

$$A(\mathrm{B}\overline{\mathrm{B}}) = r_{\mathrm{B}}(\rho) A(\mathrm{p}\overline{\mathrm{p}}) \tag{1}$$

with $r_\Lambda \cong -\frac{3}{2}\ \frac{1+2\rho}{4+\rho}$ and $r_{\Sigma^0} \cong -\frac{1}{2}\ \frac{5+2\rho}{4+\rho}$, ρ being the d/u ratio of the proton form factors: $\rho = F^{d,p}/F^{u,p}$ [5].

2 Kinematics

The production of baryon-antibaryon pairs proceeds via the process
$\mathrm{e}^+\ (\mathrm{P}_1) + \mathrm{e}^-\ (\mathrm{P}_2) \to \mathrm{e}^+\ (\mathrm{P}'_1) + \mathrm{e}^-\ (\mathrm{P}'_2) + \gamma\ (\mathrm{q}_1) + \gamma\ (\mathrm{q}_2) \to$
$\mathrm{e}^+\ (\mathrm{P}'_1) + \mathrm{e}^-\ (\mathrm{P}'_2) + \mathrm{B}\ (\mathrm{q}'_1) + \overline{\mathrm{B}}\ (\mathrm{q}'_2)$ (P_i, q_i are four-momentum vectors, Fig. 2 left). The four-momentum transfer of the virtual photons is given by $\mathrm{q}_i^2 = -\ \mathrm{Q}_i^2 = (\mathrm{P}_i\ -\ \mathrm{P}'_i)^2$.

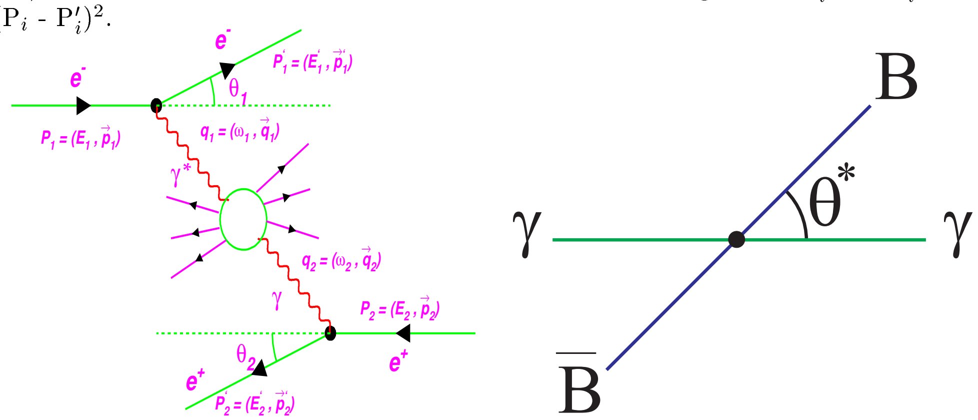

Figure 2. Definition of the kinematical variables in the two-photon reaction (left). Definition of the scattering angle Θ^* in the $\gamma\gamma$ center of mass frame (right).

The $\gamma\gamma$ c.m.s. energy $\mathrm{W}_{\gamma\gamma}$ is obtained either from the two four-momentum vectors of the γ's in the case of tagged reactions or - as is the case here - from the invariant mass of the exclusive, hadronic system. The data are analyzed only in the region of $|\cos\Theta^*| < 0.6$ (Fig. 2 right) for which theoretical predictions exist and where the detector acceptance is good.

3 Selection of $\mathrm{p}\overline{\mathrm{p}}$ Pairs

In the following, the selection of exclusive $\mathrm{p}\overline{\mathrm{p}}$ pair events in the L3 experiment will be described [6]. First, events with two well reconstructed tracks of opposite charge are selected. Antiprotons are separated from e^-, μ^- and π^- or K^- with three neural networks. The input nodes for each neural network are the momentum, the probability of the proton mass hypothesis based on the dE/dx measurement, the shape of the associated energy deposition in the electromagnetic calorimeter and the ratio of the transverse energy to the transverse momentum, E_t/p_t. To reduce the two orders of magnitude higher background from $e^+e^- \to e^+e^-e^+e^-$ further, the ratio E_t/p_t of the proton candidates after the $\overline{p}$ selection is required to be less than 0.6 (Fig. 3 left).

To select exclusive $\gamma\gamma \to p\overline{p}$ events, no photons are allowed and the square of the total sum of the proton-antiproton pair, $(\sum p_t)^2$, must be less than 0.1 GeV^2. On the right of Fig. 3 the effective mass of the selected $p\overline{p}$ events is shown. Due to the limited selection efficiency near threshold, the data are restricted to $W_{\gamma\gamma} >$ 2.1 GeV yielding 938 events.

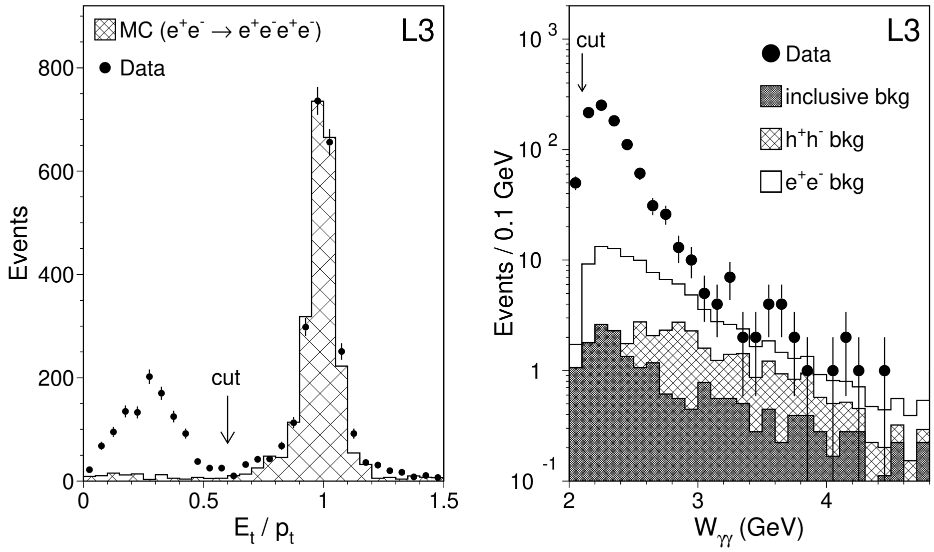

Figure 3. The ratio between the transverse energy deposited in the electromagnetic calorimeter, E_t, and the transverse momentum, p_t, for the proton candidates after the antiproton selection (left). The effective mass of the $p\overline{p}$ pair, $W_{\gamma\gamma}$, for the 989 selected events (right).

Since the $\sqrt{s}$ dependence is very small, the data are combined into one $\sqrt{s}$ bin at $< \sqrt{s} >$ = 197 GeV, yielding a cross section within $|\cos\Theta^*| < 0.6$ and 2.1 GeV $< W_{\gamma\gamma} <$ 4.5 GeV of

$$\sigma(e^+e^- \to e^+e^-p\overline{p}) = (26.7 \pm 0.9 \pm 2.7) \text{ pb}$$

Finally, the differential cross section for real photon-photon collisions $d\sigma(\gamma\gamma \to p\overline{p})/d|\cos\Theta^*|$ is obtained by using the two-photon luminosity function with a GVDM form factor given by the analytical program GALUGA [9].

4 Production of $p\bar{p}$ pairs

In Fig. 4 left, the cross section $\sigma(\gamma\gamma\rightarrow p\bar{p})$ from the L3 experiment is compared to data from the OPAL [10], CLEO [11] and VENUS [12] experiment. The L3 data agree with the earlier data and extend the $W_{\gamma\gamma}$ range. In Fig. 4 right, the L3 data are compared to the three-quark model and to the quark-diquark model. As anticipated in the introduction, the predictions of the three-quark model are about one order of magnitude below the data while the quark-diquark model describes the data quite well.

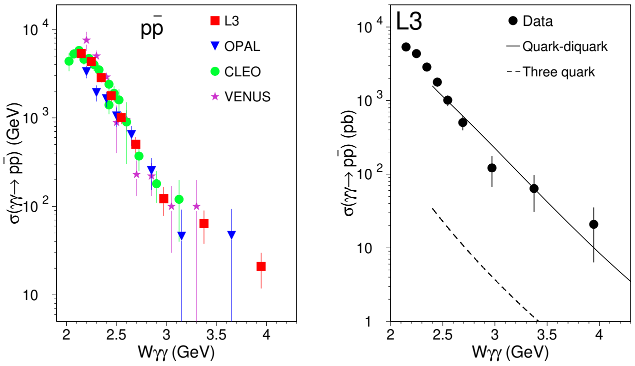

Figure 4. The $\gamma\gamma\rightarrow p\bar{p}$ cross sections as a function of $W_{\gamma\gamma}$ for $|\cos\Theta^*| < 0.6$. Comparison of the data from L3, OPAL, CLEO and VENUS (left). Comparison of the L3 data to the three-quark model calculation [2] and to the recent quark-diquark model prediction [7], available for $W_{\gamma\gamma} > 2.5$ GeV (right). Statistical and systematic uncertainties are added in quadrature.

For further comparison to the quark-diquark model the L3 cross section is shown as a function of $|\cos\Theta^*|$ for three bins of $W_{\gamma\gamma}$ together with the CLEO data for the first two $W_{\gamma\gamma}$ bins (Fig. 5). The angular dependence of $\sigma(\gamma\gamma\rightarrow p\bar{p})$ changes drastically over this $W_{\gamma\gamma}$ range. Only above $W_{\gamma\gamma}> 2.5$ GeV, the quark-diquark model starts to describe the data (as expected). Data from the Belle [13] experiment exhibit a similar behavior.

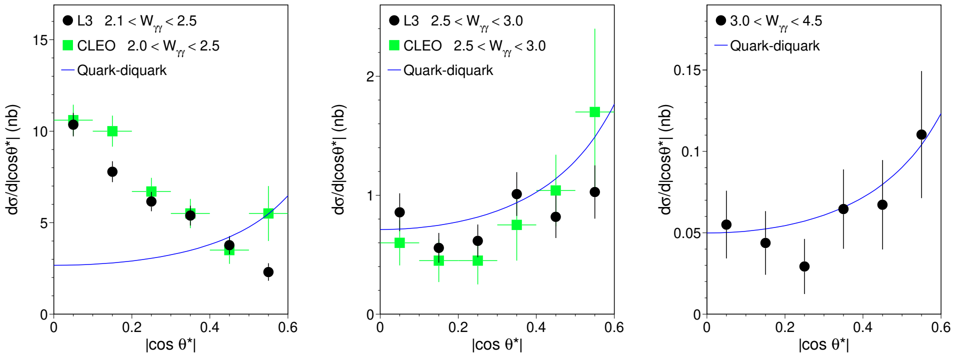

Figure 5. The differential cross section as a function of $|\cos\theta^*|$ for $2.1 < W_{\gamma\gamma} < 2.5$ GeV (left), $2.5 < W_{\gamma\gamma} < 3.0$ GeV (center) and $3.0 < W_{\gamma\gamma} < 4.5$ GeV (right). The data are compared to the predictions of the quark-diquark model [7,8].

5 Strange baryon-antibaryon pairs

The selection of $\Lambda\overline{\Lambda}$ and $\Sigma^0\overline{\Sigma^0}$ pairs in the L3 data [14] first requires four charged tracks with a net charge of zero and two secondary vertices originating from the Λ and $\overline{\Lambda}$ decays. Protons and antiprotons are selected from the dE/dx measurement and from the ratio of the transverse energy in the e.m. calorimeter to the transverse momentum, E_t/p_t. Like in the $p\overline{p}$ case, only events within $|\cos\Theta^*| < 0.6$ are retained. On the left of Fig. 6 the invariant mass of the 66 inclusive $\Lambda\overline{\Lambda}$ candidates is shown. The selection of $\Sigma^0\overline{\Sigma^0}$ events combines Λ and $\overline{\Lambda}$ candidates with photons. The mass difference $\Delta m = m(p\pi\gamma) - m(p\pi)$ must be $47 \text{ MeV} < \Delta \text{ m} < 107$ MeV (Fig. 6 right). The relative proportions of $\Lambda\overline{\Lambda}$ and $\Sigma^0\overline{\Sigma^0}$ final states is obtained in a constrained likelihood fit, yielding 12.5 ± 0.18 $\Lambda\overline{\Lambda}$ events and 20.5 ± 6.5 $\Sigma^0\overline{\Sigma^0}$ events. The fraction of $\Lambda\overline{\Sigma^0} + \overline{\Lambda}\Sigma^0$ is measured to be compatible with zero.

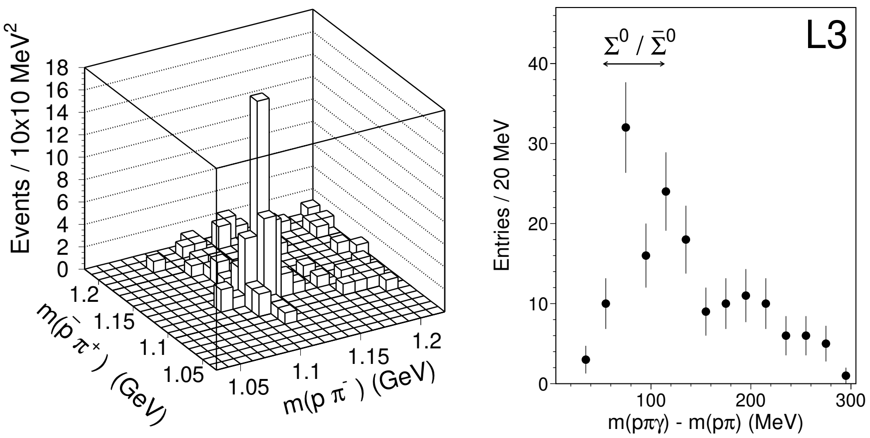

Figure 6. The scatter plot of $m(\overline{p}\pi^+)$ versus $m(p\pi^-)$ (left). Distribution of the mass difference between the $\Lambda\gamma$ ($p\pi\gamma$) and the Λ ($p\pi$) systems.

The cross sections $\sigma(\gamma\gamma \to \Lambda\overline{\Lambda})$ and $\sigma(\gamma\gamma \to \Sigma^0\overline{\Sigma^0})$ for real photons is again obtained with the same procedure [9] as in the $p\overline{p}$ case. In Fig. 7 left the L3 data are compared to CLEO data [15]. The $W_{\gamma\gamma}$ dependence of the $\Lambda\overline{\Lambda}$ cross section is less steep for the L3 data and more compatible with the predictions of the quark-diquark model. The predictions of the three-quark model are again an order of magnitude too low. The $\Sigma^0\overline{\Sigma^0}$ cross section from L3 (Fig. 7 center) corroborates the last statement and the upper limit obtained for $\Lambda\overline{\Sigma^0} + \overline{\Lambda}\Sigma^0$ (Fig. 7 right) is compatible with the quark-diquark predictions.

Finally, in Fig. 8 the same data are compared to the predictions of the handbag model which agree within theoretical uncertainties with the data.

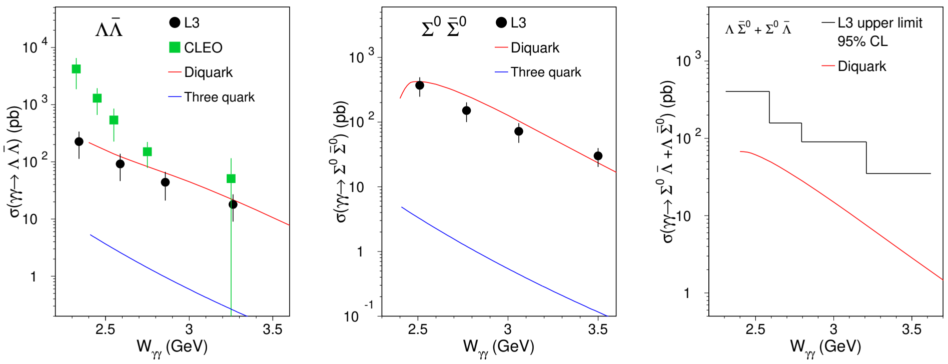

Figure 7. The cross sections $\gamma\gamma \to \Lambda\overline{\Lambda}$ (left), $\gamma\gamma \to \Sigma^0\overline{\Sigma^0}$ (center) and $\gamma\gamma \to \Sigma^0\overline{\Lambda}$ and $\gamma\gamma \to \Lambda\overline{\Sigma^0}$ (right) compared to the predictions of the three-quark and to the quark-diquark model.

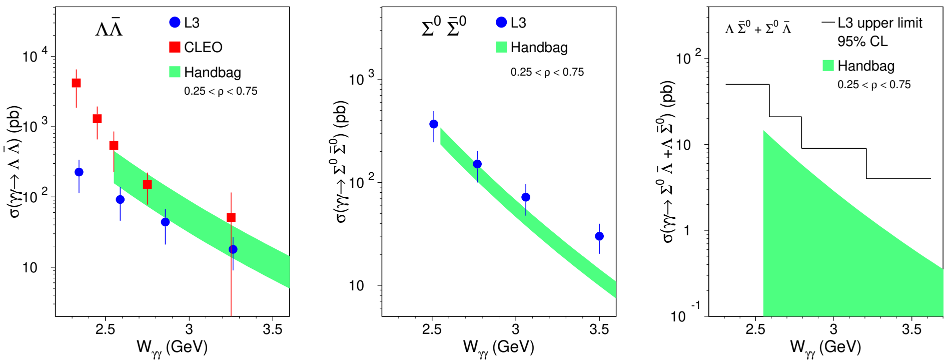

Figure 8. The cross sections $\gamma\gamma \to \Lambda\overline{\Lambda}$ (left), $\gamma\gamma \to \Sigma^0\overline{\Sigma^0}$ (center) and $\gamma\gamma \to \Sigma^0\overline{\Lambda}$ and $\gamma\gamma \to \Lambda\overline{\Sigma^0}$ (right) compared to the predictions of the handbag model.

6 Conclusions

The production of exclusive baryon-antibaryon pairs in two-photon collisions shows that present predictions of the three-quark model are in all cases much too low. The quark-diquark and the handbag model describe the data for $W_{\gamma\gamma} > 2.5$ GeV reasonably well. In the future, much higher statistics can be expected from the BELLE experiment.

7 Acknowledgments

I would like to thank my colleagues from the L3 two-photon group, Bertrand Echenard, John Field and Maria Kienzle, for their help and advice.

References

1. S. J. Brodsky and J. P. Lepage, Phys. Rev. **D 22** (1980) 2157.
2. G. Farrar, E. Maina and F. Neri, Nucl. Phys. **B 259** (1985) 702; Nucl. Phys. **B 263** (1986) 746.
3. D. Millers and J. F. Gunion, Phys. Rev. **D 34** (1986) 2657.
4. M. Anselmino, P. Kroll and W. Schweiger, Int. Jour. Mod. Phys. **A 4** (1989) 5213.
5. M. Diehl, P. Kroll and C. Vogt, Eur. Phys. J. **C26** (2003) 567.
6. P. Achard et al., Phys. Lett. **B 571** (2003) 11;
   P. Achard et al., Phys. Lett. **B 536** (2002) 24.
7. C. F. Berger, B. Lechner and W. Schweiger, Fizika **B 8** (1999) 371;
   C. F. Berger and W. Schweiger, preprint hep-ph/0212066 (2002).
8. C. F. Berger, private communication for the quark-diquark predictions at $W_{\gamma\gamma} < 2.5$ GeV.
9. G. A. Schuler, preprint CERN-TH/96-297 (1996).
10. G. Abbiendi et al., Eur. Phys. J. **C 28** (2003) 45.
11. M. Artuso et al., Phys. Rev. **D 50** (1994) 5484.
12. H. Hamasaki et al., Phys. Lett. **B 407** (1997) 185.
13. C. C. Kuo et al., Nucl. Phys. **A 721** (2003) 817.
14. P. Achard et al., Phys. Lett. **B 536** (2002) 24.
15. S. Anderson et al., Phys. Rev. **D 56** (1997) 2485.